

Artifacts resulting from imaging in scattering media: a theoretical prediction

Alexander Rohrbach

Laboratory for Bio- and Nano-Photonics, Department of Microsystems Engineering-IMTEK, University of Freiburg, Centre for Biological Signalling Studies (bloss), University of Freiburg, Germany (rohrbach@imtek.de)

Received April 13, 2009; revised July 10, 2009; accepted July 30, 2009;
 posted August 20, 2009 (Doc. ID 110010); published September 30, 2009

Scattering of illumination light from a laser is a severe problem especially when imaging in thick media. Although this effect occurs in nearly every imaging process, it can be well perceived and analyzed in configurations where the optical axes for illumination and detection are perpendicular to each other. In this paper I present a theoretical perspective of how to extend the point-spread function arithmetic from ideal imaging to realistic imaging including ghost images. These ghost images are generated by scattered light and are low-correlated with the ideal image. Numerical simulations of the propagation of four different types of illumination beams through a cluster of spheres illustrate the effects of inhomogeneous object illumination. Clear differences between a conventional plane-wave illumination, a static light-sheet, and a laterally scanned Gaussian beam, but also relative to a scanned Bessel beam, can be observed. © 2009 Optical Society of America

OCIS codes: 110.2990, 110.6880, 110.7050, 180.6900, 290.2745, 290.4210.

Imaging in thick media, such as cell clusters or even whole organisms [1], has conspicuously gained interest, since division and signaling of living cells need to be investigated in the surrounding of other cells communicating with each other [2]. However, imaging in several hundred micrometer-thick tissue requires new illumination and detection optics on the one hand, but also novel concepts and a more detailed analysis of the interaction of light with matter on the other hand. With this I refer to the propagation of light through matter and the accompanying scattering of light, which is usually hardly controllable and, through beam spreading, leads to a loss of image resolution and contrast. Furthermore it can also enhance or block the illumination of nearby scatterers and thus produce strong artifacts in images. These artifacts can be summarized in the term low-correlated “ghost image,” which is superposed on the ideal image. These ghost images are produced with nearly every microscopy technique, but can be very well perceived and analyzed with techniques where illumination and detection axes are oriented at 90° to each other [3–6]. On the theoretical or analytical side, the well-established concept from linear system theory, i.e., convolution of the object with the point-spread function (PSF) [7], fails in the case of strong scattering or, at least, needs to be extended.

In this Letter I present an idea of how to tackle the problem of imaging in thick media by extending the concept of PSF convolution by including terms that describe the unwanted scattered illumination light. This approach allows categorizing and estimating the ghost image artifacts. Wave optical simulations manifest and illustrate both the problem and the PSF concept for four different illumination types.

The principal lens arrangement of a selective plane illumination microscope (SPIM) [1] is shown in Fig. 1(a), where the illumination objective weakly focuses coherent light along z into a specimen exciting one-

photon fluorescence in a linear process. An illumination light-sheet in the focal plane of the detection lens (xz plane) is realized by either focusing light only vertically along y , or by scanning a rotationally symmetric focused beam in the x direction. Fluorescent light is then collected in the y direction by a high-NA detection objective. A virtual magnification from the inside of the specimen shows how a homogeneous illuminating wave becomes quickly inhomogeneous while propagating through a cluster of spheres [Fig. 1(b)].

The intensity PSFs for detection and illumination are denoted as $h_{det}(\mathbf{r})$ and $h_{ill}(\mathbf{r})$, where the latter can be separated into an incident, i.e., nonscattered, and a scattered part $h_{inc}(\mathbf{r})$ and $h_{sca}(\mathbf{r})$, such that

$$h_{ill}(\mathbf{r}) = |\mathbf{E}_{tot}(\mathbf{r})|^2 = |\mathbf{E}_{inc}(\mathbf{r}) + \mathbf{E}_{sca}(\mathbf{r})|^2 = h_{inc}(\mathbf{r}) + h_{sca}(\mathbf{r}), \quad (1)$$

where $h_{sca}(\mathbf{r}) = |\mathbf{E}_{sca}(\mathbf{r})|^2 + 2\text{Re}\{\mathbf{E}_{inc}(\mathbf{r}) \cdot \mathbf{E}_{sca}(\mathbf{r})^*\}$ includes both incoherent and coherent terms from the

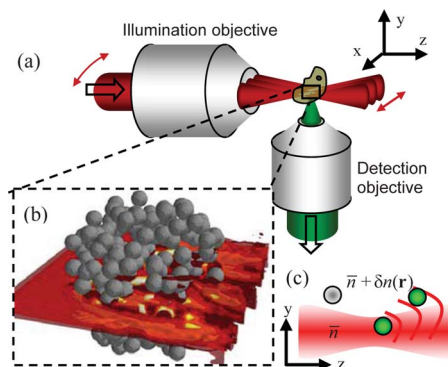


Fig. 1. (Color online) (a) Illumination along z and detection in y in a 90° arrangement. (b) Magnification of a light-sheet propagating through a cluster of spheres. (c) Scheme for illumination and scattering at spheres with index $n(r)$. Illuminated spheres are green.

incident and scattered electric fields \mathbf{E}_{inc} and \mathbf{E}_{sca} . Remarkably, $h_{sca}(\mathbf{r})$ can become negative. The total field \mathbf{E}_{tot} propagating through the sample can be described numerically by a beam propagation method (BPM) [8], with the angular spectrum at distance $z + dz$,

$$\tilde{\mathbf{E}}_{tot}(k_x, k_y, z + dz) = FT[\mathbf{E}_{tot}(x, y, z) \times e^{(-ik_0 \cdot \delta n(x, y, z) \cdot dz)}] \times e^{-i \cdot dz \cdot \sqrt{(k_0 \cdot \bar{n})^2 - k_x^2 - k_y^2}} \quad (2)$$

Here $FT[.]$ denotes the Fourier transform in x and y , and $k_0 = 2\pi/\lambda$ is the vacuum wavenumber. The space dependent refractive index $n(\mathbf{r}) = \bar{n} + \delta n(\mathbf{r})$ changes by $\delta n(\mathbf{r}) < \delta n_{max}$ around the mean value \bar{n} , typically defined by the index of the scatterer's environment [see Fig. 1(c)]. In the simplest approach one assumes a fluorophore distribution $C_1(\mathbf{r}) = C_0 \cdot \delta n(\mathbf{r})$, where scatterers with index $n(\mathbf{r}) > \bar{n}$ are stained. In this study a distribution $C_2(\mathbf{r}) = C_0 \cdot (1 - \delta n(\mathbf{r})/\delta n_{max})$ was taken, where the scatterer's environment is labeled, enabling imaging of scattered light.

In conventional, nonconfocal imaging an intensity image $b(\mathbf{r})$ is obtained by the illuminated part of the object $h_{ill}(\mathbf{r}) \cdot C(\mathbf{r})$ convolved (symbol $*$) with the detection PSF $h_{det}(\mathbf{r})$:

$$b(\mathbf{r}) = \{[h_{inc}(\mathbf{r}) + h_{sca}(\mathbf{r})] \cdot C(\mathbf{r})\} * h_{det}(\mathbf{r}). \quad (3)$$

According to Eq. (3) a real image can be decomposed into an ideal image and a ghost image, $b_{real}(\mathbf{r}) = b_{ideal}(\mathbf{r}) + b_{ghost}(\mathbf{r})$, where the latter results from illumination with scattered, interfering light:

$$b_{ghost}(x, y_0, z) = [h_{sca}(\mathbf{r}) \cdot C(\mathbf{r})] * h_{det}(\mathbf{r})|_{y=y_0}. \quad (4)$$

In contrast to ghost images that are reflected or deflected from defined surfaces (e.g., beam splitters or gratings), here the correlation between b_{ideal} and b_{ghost} quickly falls off to small values with increasing distance z , i.e., $b_{ideal}(\mathbf{r}) * b_{ghost}(-\mathbf{r}) = \text{const}$.

The relative energy Q inherent in the ghost image is estimated by normalizing $b_{ghost}(x, z)$. Since relevant image information is in its nonzero spectral components, one can normalize an image b by its dynamic range ($b_{max} - b_{min}$). Instead of considering single high or low pixels, it is more useful to normalize by 2 times the standard deviation $\sigma(b(x, z))$ of the image intensity, such that the normalized ghost image and the relative energy Q are defined as

$$Q = A^{-1} \cdot \int |\hat{b}_{ghost}| dA, \quad \hat{b}_{ghost} = b_{ghost}/2\sigma(b_{ideal}). \quad (5)$$

$Q(y_0)$ from plane y_0 can be interpreted through a single quality value, which is obtained by averaging the modulus of the normalized $\hat{b}_{ghost}(x, y_0, z)$ over the image area A . $\hat{b}_{ghost}(x, y_0, z)$ provides a map of how this error spreads with propagation distance z . The smaller Q , the less the image is deteriorated by the ghost image as a result of a nonnegligible $h_{sca}(\mathbf{r})$. These effects are illustrated in the following by calculating both the image $b_{real}(\mathbf{r})$, with light scattered

by the index variations $\delta n(\mathbf{r}) \neq 0$, relative to the image $b_{ideal}(\mathbf{r})$ with no scattering [$\delta n(\mathbf{r}) = 0$; see Eq. (2)].

A similar analysis can be performed by mapping the relative error $R_{ill}(x, y_0, z) = h_{sca}(x, y_0, z)/h_{inc}(x, y_0, z)$ of the real illumination PSF ($h_{sca} + h_{inc}$) relative to the ideal PSF h_{inc} , produced solely by the illumination of the objects with $\delta n(\mathbf{r}) \neq 0$. The relative illumination energy $Q_{ill}(y_0) = A^{-1} \cdot \int |R_{ill}| dA$ is defined equivalently to Eq. (5).

Numerical Simulation A near-experiment situation is the propagation of light at $\lambda = 0.5 \mu\text{m}$ through a spherical cluster (diameter $2R \approx 11 \mu\text{m}$) of 250 glass spheres ($n = 1.43$) with $2a = 1 \mu\text{m}$ in diameter with $\delta n(\mathbf{r}) = \delta n_{max} = 0.1$ embedded in a gel with $\bar{n} = 1.33$. The vectorial BPM used with 256^2 -FFTs (256 pixel $\equiv 16 \mu\text{m}$) considers realistic forward, but no backscattering. A fluorophore distribution $C_2(\mathbf{r})$ was chosen to be imaged by an aplanatic water immersion lens with $\text{NA}_{det} = 0.67 \cdot \bar{n} = 0.9$. Four different types of coherent illuminations were tested: Type A is a plane wave propagating along y in wide-field mode through the detection lens; the other three propagate in 90° arrangement along z . Type B is a static light-sheet focused only in y with $\text{NA}_{ill} = 0.2 \cdot \bar{n}$. Type C is an x -laterally scanned Gaussian beam with $\text{NA}_{ill} = 0.2 \cdot \bar{n}$. Type D is a scanned Bessel beam with $\text{NA}_{ill} = 0.4 \cdot \bar{n}$ and ring aperture ratio $\varepsilon = 0.8$. Cross sections of the resulting light-sheets are shown in Fig. 2. The three light-sheets have comparable depths of field of more than $\Delta z \approx 30 \mu\text{m} > 2R$.

Results Simulation results are illustrated in Fig. 3 for all four illumination modes (Types A to D). The cross sections of the illumination intensities $h_{ill}(x, z) \cdot C_2(x, z)$ in column 1 show the strong variations due to scattering in Types A to C but smaller variations for the Bessel Type D. This is further manifested by the error maps $R_{ill}(x, y_0, z)$ in column 2 and the total mean errors Q_{ill} , which are $\approx 30\%$ for Types A to C but only $Q_{ill} = 21\%$ for Type D. The white spots from the spheres indicate not-a-number (NaN) and arise from zeros in the denominator of $R_{ill}(x, y_0, z) = h_{sca}(x, y_0, z)/h_{inc}(x, y_0, z)$. The real image slices $b_{real}(x, z)$ one would observe in a microscope are obtained according to Eq. (3) and are shown in column 3, while the ideal image slices $b_{ideal}(x, z)$, neglecting the scattering, are shown in column 4. In columns 3 and 4 the minimum b_{min} has been subtracted in the picture. However, the contrast in the

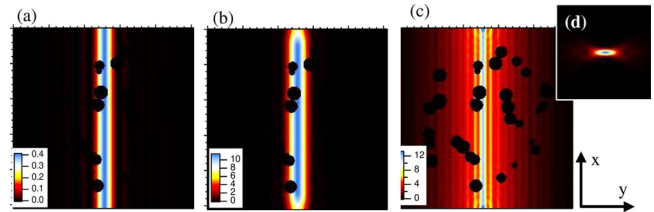


Fig. 2. (Color online) Cross sections of unstained spheres and of ideal light-sheets in the center of the sphere cluster. (a) Gaussian beam focused only in y at $\text{NA} = 0.26$, (b) focused Gaussian beam scanned in x at $\text{NA} = 0.2$, (c) focused Bessel beam scanned in x at $\text{NA} = 0.52$, (d) detection PSF $h_{det}(x, y)$ with $\text{NA} = 0.9$ is shown for size comparison.

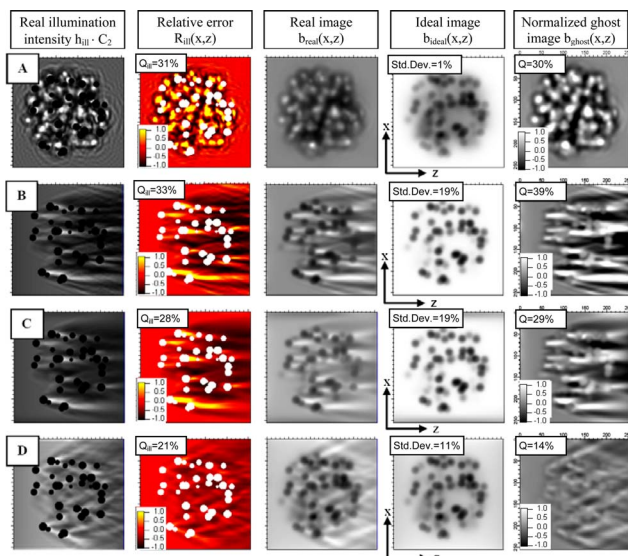


Fig. 3. (Color online) Illumination and imaging with a plane wave (Type A), a cylindrical beam (Type B), a scanned Gaussian beam (Type C), and a scanned Bessel beam (Type D).

ideal image, expressed by the standard deviation $\sigma(b_{ideal}(x, z))$, reveals the expected very weak contrast ($\sigma \approx 1\%$) for the wide-field image (Type A), and a good contrast ($\sigma = 19\%$) due to sectioning for both the cylindrical beam and the scanning Gaussian beam (Types B and C). The ring system around the scanned Bessel beam manifests as an image blur and thus reduces the contrast ($\sigma = 11\%$). Column 5 shows the normalized ghost images $\hat{b}_{ghost}(x, y_0, z)$ with corresponding mean energies $Q(y_0)$ per plane y_0 , which are $Q = 0.3, 0.4,$ and 0.3 for Types A, B, and C but only $Q = 0.14$ for Type D. The Bessel beam thus produced the least pronounced ghost image [see Eqs. (4) and (5)].

Discussion and Conclusion The procedure to estimate the quality of an image according to Eq. (5) reflects the amount of scattering and the generation of an ghost image [see Eq. (4)], which results from the illumination of fluorophores by scattered light and the interference of scattered and unscattered light, i.e., $|\mathbf{E}_{sca}|^2 + 2\text{Re}\{\mathbf{E}_{inc} \cdot \mathbf{E}_{sca}^*\}$. In this study the image contrast is degraded by scattering of illumination light. Scattering of fluorescence light on the detection side was not considered.

However, the strong differences in the ghost images point out the importance of the object illumination, which on the one hand is different between a scanning beam approach and static light-sheet, or in other words, between a spatially incoherent and a coherent illumination in lateral x direction (see also [5,6]). Since the scanning type suppresses the term $\text{Re}\{\mathbf{E}_{inc}(x) \cdot \mathbf{E}_{sca}^*(x)\}$ in the illumination PSF $h_{ill}(x)$, less scattering is visible on average. However, in both cases intensity changes of more than 100% can partially occur, making objects much brighter or dimmer. On the other hand a scanned Bessel beam reveals tremendously reduced scattering, which is favored by the higher focusing angle at the same depth of field

($\text{NA}_{ill}^{Bessel} \approx 2 \cdot \text{NA}_{ill}^{Gauss}$) and the ability of self-reconstruction, which has been proven several times in free space [9], i.e., without scatterers. Nevertheless, the ring system around the narrow main peak of the Bessel beam, which can be controlled in its strength by the ε value (here $\varepsilon = 0.8$), also illuminates out of focus planes and thereby reduces the image contrast. It is important to emphasize that similar scattering effects and ghost images are produced in various microscopies with coherent illumination, i.e., also in confocal microscopy.

How trustworthy is the simulation? First, the (vectorial) BPM is a useful calculation method, when arbitrary index distributions $n(\mathbf{r}) = \bar{n} + \delta n(\mathbf{r})$ with small $\delta n(\mathbf{r})$ are considered and when the propagation angle is not too large ($\sin \alpha < 0.5$), as in our study. However, backscattering is neglected and is put into the forward scattered energy, which increases the overall scattering and the strength of ghost images. This could be compensated for by an adequate imaginary refractive index of the scatterers. Second, the $2R = 11 \mu\text{m}$ large cluster of 250 randomly distributed, glass spheres [$n(\mathbf{r}) = \bar{n} + \delta n(\mathbf{r}) = 1.33 + 0.1$] has a volume ratio of $250 a^3/R^3 \approx 0.2$ and can be considered to be not too different from biological matter. Larger clusters will further increase the problem with scattering and ghost images.

The message of this study is that scattering effects are often strong, can be well visualized in SPIM-like configurations and may lead to a significantly wrong interpretation of microscopic data. The resulting disturbance can be summarized in a ghost image, which is low-correlated with ideal image and which is superposed to the ideal image. In experiments, a first step must be to analyze scattering effects by comparing images with different illumination directions, which is easily possible in SPIM-like configurations, but also possible in classical microscopes, e.g., by blocking different parts in the back focal plane of the illumination lens. A second step could be to adapt the angular spectrum of the illumination beam to the specimen index distribution by spatial light modulators. I think the realization of such microscopes is just a question of some years.

I thank Florian Fahrbach, Lars Friedrich, Dr. Olaf Ronneberger, and Dr. Helmut Lippert for helpful discussions and a thorough reading of the manuscript.

References

1. J. Huisken, J. Swoger, F. Del Bene, J. Wittbrodt, and E. H. K. Stelzer, *Science* **305**, 1007 (2004).
2. A. Abbott, *Nature* **424**, 870 (2003).
3. A. H. Voie, D. H. Burns, and F. A. Spelman, *J. Microsc.-Oxford* **170**, 229 (1993).
4. A. Rohrbach, *Biophys. J.* **78**, 2641 (2000).
5. J. Huisken and D. Y. R. Stainier, *Opt. Lett.* **32**, 2608 (2007).
6. P. J. Keller, A. D. Schmidt, J. Wittbrodt, and E. H. K. Stelzer, *Science* **322**, 1065 (2008).
7. N. Streibl, *J. Opt. Soc. Am. A* **2**, 121 (1985).
8. M. D. Feit and J. A. Fleck, *Appl. Opt.* **17**, 3990 (1978).
9. D. McGloin and K. Dholakia, *Contemp. Phys.* **46**, 15 (2005).